Title: Valence-Induced Jumps in Coacervate Properties

One-Sentence Summary: There is a jump in the modulus and viscosity of coacervates made from charged (bio)polymers and small molecules when valency increases from three to four.

Authors: Mo Yang¹, Zachary A. Digby¹, Yuhui Chen¹, Joseph B. Schlenoff¹*

Affiliations:

5

10

15

20

25

30

35

40

¹Department of Chemistry and Biochemistry, Florida State University; Tallahassee, FL 32306 USA

*Corresponding author. Email: jschlenoff@fsu.edu

Abstract: Spontaneous phase separation, or coacervation, of oppositely-charged macromolecules is a powerful and ubiquitous mechanism for the assembly of natural and synthetic materials. Two critical triggering phenomena in coacervation science and technology are highlighted here. The first is the transition from one (mixed) to two (separated) phases of polyelectrolytes coacervated with small molecules upon the addition of one or two charges per molecule. The second is a large jump in coacervate modulus and viscosity mediated by the addition of just one additional charge to a 3-charged system. This previously-unknown viscoelastic transition is relevant to those aspects of disease states that are characterized by abnormal mechanical properties and irreversible assembly.

Introduction:

The term "coacervation" was coined by Bungenberg de Jong to describe the spontaneous separation of a homogeneous liquid mixture of biopolymers into two or more distinct phases.(1) This type of liquid-liquid phase separation, LLPS, was soon proposed to be one of the mechanisms used to organize and compartmentalize living systems without requiring cell membranes.(2, 3) Interest in membrane-less organelles has intensified with the discovery of an increasing number of functional droplets within cells and the participation of intrinsically disordered proteins in their formation.(4-6) The nucleolus, an early example of a membrane-less organelle, is now known to comprise RNA and proteins with intrinsically disordered regions which undergo LLPS in vitro.(7)

A focus on biological coacervation is paralleled by extensive research in the basic physical chemistry and materials science of the products of LLPS.(8-11) Unfortunately, research on biological and synthetic coacervates(12-17) have followed largely separate tracks, though the underlying science is similar. Solid-like products, more common for synthetic systems, are often termed "complexes."(15, 16, 18) For these, it is possible to access the liquid state by doping with salt or changing other physical variables such as pH.(19, 20) Potential driving forces for coacervation/complexation include a number of physical interactions such as charge pairing, or "electrostatics," between oppositely-charged units.(21) Charge pairing, coupled to and weakened

10

15

20

25

30

by salt counterions, is driven by the entropic release of counterions. (22) Enthalpic contributions from hydrogen bonding and hydrophobic interactions (23) manifest themselves as upper- or lower critical solution temperatures. (24) Some of the strongest interactions involve arginine - capable of both hydrogen-bonding and charge pairing. (25)

Multivalent interactions lead to net free energies that scale with the number of interacting groups. (26-28) Coacervation in the synthetic and bio- realms is typically demonstrated by association between macromolecules, notably RNA as the negative binding partner. However, Mann and coworkers (29) and Keating and coworkers (30-33) have demonstrated the potential of biotically-relevant small molecules having few charges to promote LLPS.

Coacervate formation is summarized by phase diagrams, such as those presented in Figure 1. The boundaries between phases depend principally on salt concentration, type of interacting charges,(34) number of charges and charge density. For a specific pair of coacervating polymers, added salt switches off LLPS at the so-called critical salt concentration, CSC.(35) The greater the number of charges, the higher the CSC, as illustrated for polymer/polymer coacervates experimentally(12, 36) and by theory(37, 38). Because the CSC is typically near the apex of the phase diagram, it is often shown at the apex, but this is not necessarily the location of the CSC.(39) The sensitivity of the CSC to the number of charges increases strongly as the charge density decreases to a few per molecule. In Figure 1, coacervation in a system just above the CSC may be triggered by the addition of even one charge pair.(31)

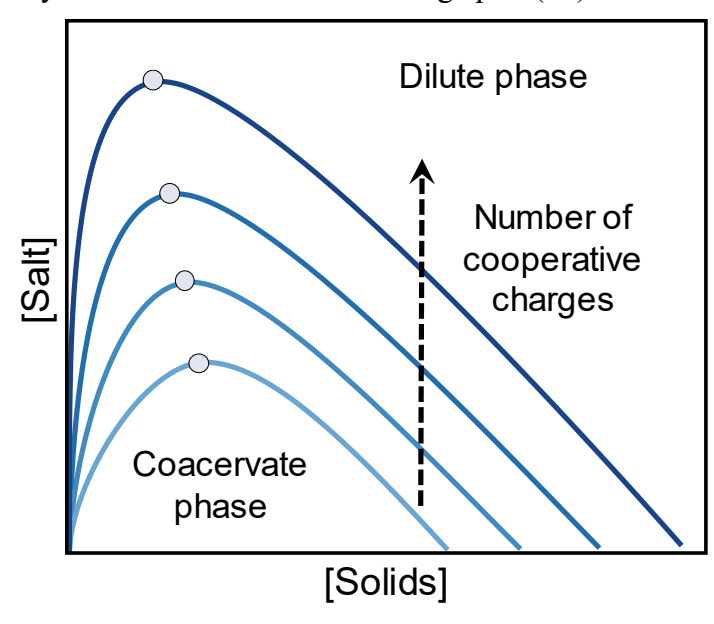


Figure 1. Phase diagram of polyelectrolyte coacervation. No LLPS occurs above the critical salt concentrations, shown by the dots, which depend on the molecular weight (or the number of charges per molecule). A larger number of charges stabilizes the coacervate against salt.

Far more is known about conditions for triggering coacervated droplets than is known about their properties, yet much prior research has highlighted the perceived importance of, for example, viscoelasticity on function (or dysfunction). Many disease states, including neurodegenerative conditions, are characterized by increases in modulus or viscosity, which enable irreversible aggregation and distinct morphology changes. (24, 40-42) Detailed measurements of materials properties (43) such as changes in viscosity (25, 44) have recently come to the forefront in attempts to understand the fundamentals of coacervation.

The present work examines two aspects of the "jumps" in the nature of coacervation. One component was macromolecular while the other remained small to further illustrate that coacervation requires only one polymeric species. The small components were selected to illustrate the effect of an increasing number of charge-pairing interactions on the formation and properties of polyelectrolyte coacervates, PECs. First, using either a synthetic system with increasing numbers of aromatic sulfonates, or a biologically relevant system with increasing numbers of phosphate groups and a polypeptide, a substantial jump in modulus and viscosity occurs for an increase from three to four charges per molecule, providing materials with solid, even glassy, properties. Second, using the phosphate/polypeptide PEC, the phase boundary in physiological salt concentration between unassociated and associated molecules is crossed with the addition of two charges by in situ hydrolysis.

Results and Discussion:

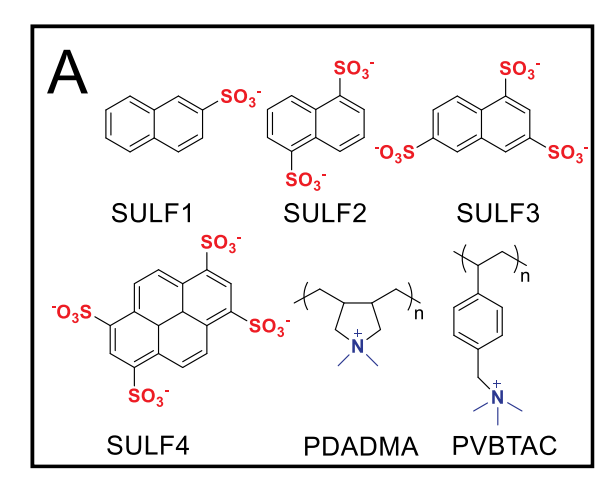
5

10

15

20

We prepared the first series of coacervates using the sulfonate/quaternary ammonium charge pair. A set of molecules bearing from 1 to 4 sulfonates each is shown in Figure 2A. We complexed these with the polycation poly(diallyldimethylammonium), PDADMA, fractionated to provide a relatively narrow distribution of molecular weights (see Figure S1, Supporting Information). Coacervate droplets were centrifuged to yield a continuous polymer-rich phase and a "dilute" phase (see Figure 2B). While properties and composition are known to change with salt concentration, (45) in the current study we maintained [NaCl] near zero or 0.15 M.



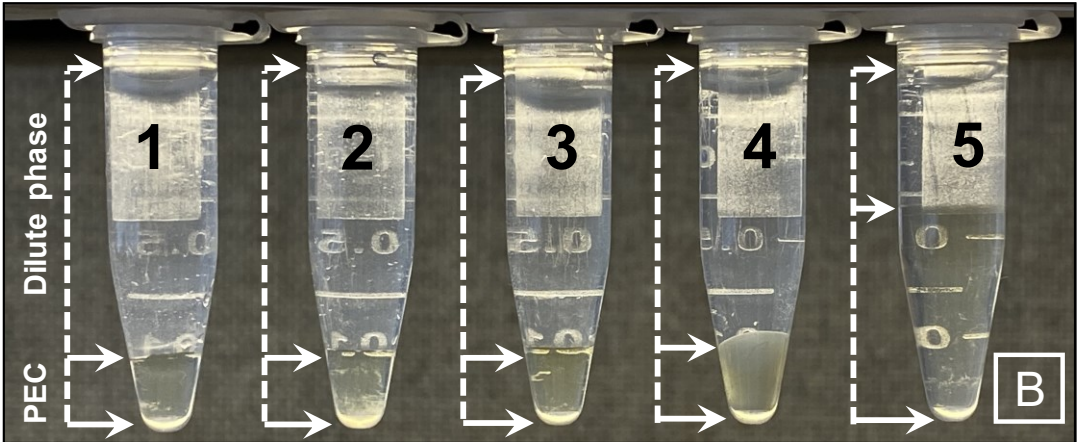


Fig. 2. Molecules used for SULF series of PECs. 2. A) small- and macromolecular charged partners used in this study; B) images of, 1, SULF1/PDADMA; 2, SULF2/PDADMA; 3,

10

15

20

25

30

35

SULF3/PDADMA; 4, SULF4/PDADMA; and 5, SCN/PDADMA coacervates (lower phase) in 1.5 mL centrifuge tubes. The upper phase is termed the "dilute phase" (indicated by the arrows).

All compositions were close to stoichiometric in terms of SO₃⁻:PDADMA⁺ charge ratios (Table 1, Supporting Information Figure S2). The water and solids content, determined by drying (Table 1), showed only a slight change in composition across the sulfonate series. The critical concentration of NaCl required to revert the 2-phase system back into one phase increased substantially with the number of sulfonates. Thus, only the SULF4/PDADMA coacervate would form at [NaCl] > 0.53 M.

While entropy provides a driving force for complex formation due to the liberation of counterions on the polymer, much of the driving force in the SULF/PDADMA series comes from the enthalpy of complexation, which increases with the number of -SO₃⁻ per molecule and illustrates the influence of binding polyvalency or cooperativity (Table 1). Interestingly, there is a jump in the enthalpy per SO₃⁻ going from SULF3 to SULF4, probably a result of the added aromaticity/hydrophobicity.

Because all hydrated coacervate phases were macroscopic, large-scale rheological measurements could be recorded to determine the viscoelastic response (VR) as a function of frequency (storage modulus, G'; loss modulus G" in Figure 3. Figure S3 in Supporting Information shows viscosity and shift factors used to perform time-temperature superposition(46)). There were relatively minor differences between the VR of coacervates made with SULF1 thru SULF3 (Figures 3A, 3B, 3C). SULF4/PDADMA exhibited a remarkable jump in modulus and a full range of frequency dependent (Figure 3D and S3) and temperature dependent (Figure S4) VR from liquidlike to rubbery to almost glassy. The (zero shear) viscosity remains virtually constant for SULF1 thru SULF3, then jumps by a factor of 160 for SULF4 (Table 2). Very little separates the SULF series of PECs in terms of composition. The only clue to the extraordinary properties of SULF4/PDADMA provided in Figure 2 is the skewed interface at the bottom of the centrifuge tube. The unusually glassy nature of a coacervate formed from a polyelectrolyte and a small molecule with just four charges is emphasized by the observation of a glass transition temperature at around room temperature for a coacervate between SULF4 and the strongly pairing polycation poly(vinylbenzyltrimethyl ammonium)/(PVBTA (Figure 4). We did not observe Tgs for the other systems, which we assumed to be below 0 °C.

Table 1. Stoichiometry, polyelectrolyte (PE) volume fraction, critical salt concentration, of SULF/PDADMA PECs, and heat of complexation determined by isothermal titration calorimetry.

Sample	Stoichiometry (SO ₃ ⁻ :PDADMA)	PE% Volume fraction	Critical NaCl concentration (M)	Total charges per SULF molecule	ΔH per SULF molecule (±100 J mol ⁻¹)	ΔH per SO ₃ - group (±100 J mol ⁻¹)
SULF1/ PDADMA	0.97:1.00	20.4	0.04	1	-950	-950
SULF2/ PDADMA	1.00:1.00	20.1	0.08	2	-5320	-2660
SULF3/ PDADMA	0.99:1.00	22.8	0.53	3	-7790	-2600

SULF4/ PDADMA	0.99:1.00	28.6	2.68	4	-23500	-5880	

Table 2. Dynamic properties of SULF/PDADMA PECs

Sample	Zero shear viscosity, η _o (±100 Pa s)	Plateau Modulus G _o (Pa)	Reptation Rate ω_{rep} (s ⁻¹)	Entanglement Rate, ω _e (s ⁻¹)
SULF1/ PDADMA	1400	25000	22	60000
SULF2/ PDADMA	1300	32000	28	70000
SULF3/ PDADMA	1300	33000	25	60000
SULF4/ PDADMA	210000	25000	0.1	890

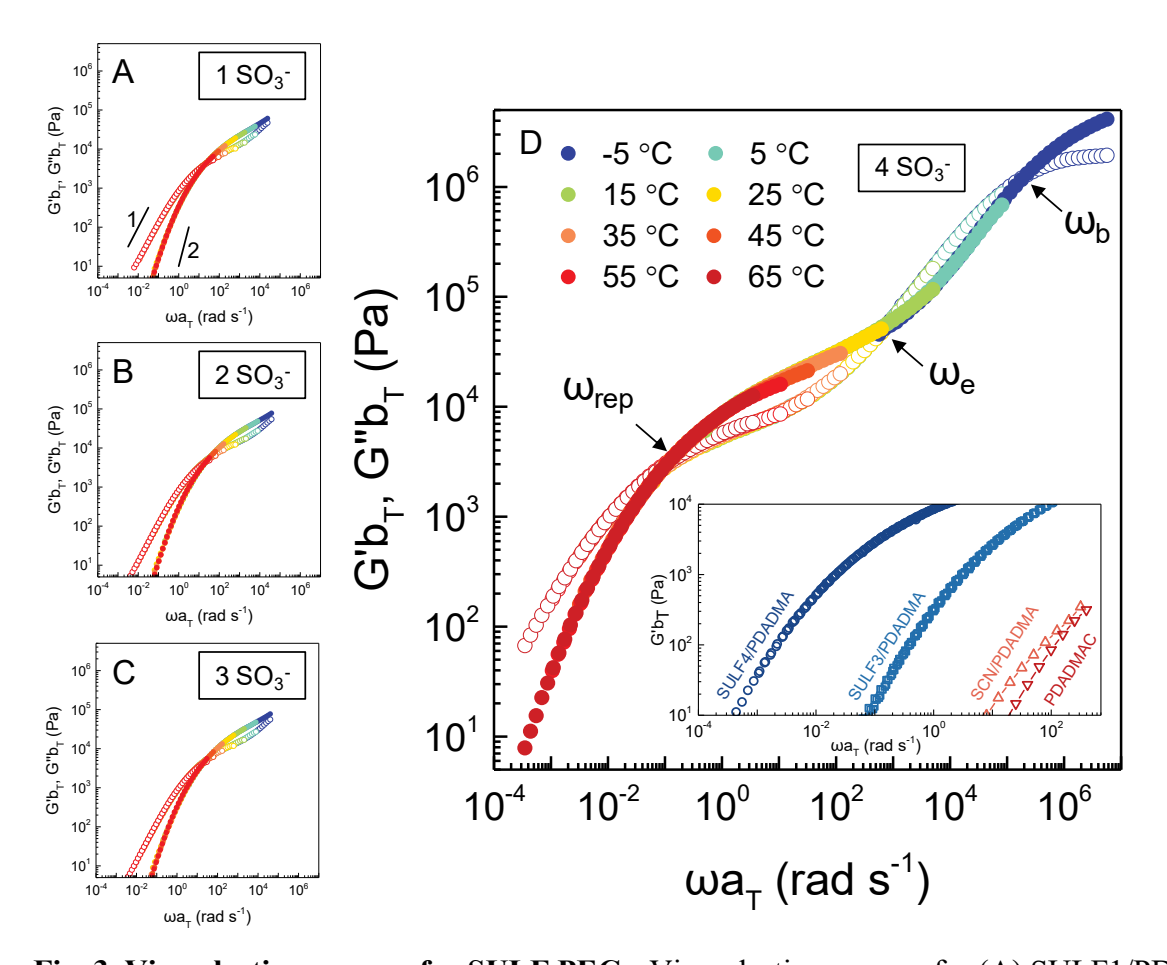


Fig. 3. Viscoelastic response for SULF PECs. Viscoelastic response for (A) SULF1/PDADMA; (B) SULF2/PDADMA; (C) SULF3/PDADMA; and (D) SULF4/PDADMA. Storage modulus G' (filled symbols) and loss modulus G' (open symbols), are shown as function of frequency, shifted from different temperatures according to time-temperature superposition with a reference

temperature of 25 °C. Inset compares G' in the terminal regime for SULF4/PDADMA, SULF3/PDADMA, SCN/PDADMA and 27.5 wt% PDADMAC solution. Characteristic relaxation rates ω_{rep} , ω_e , and ω_b are shown in D. Reference temperature 25 °C.

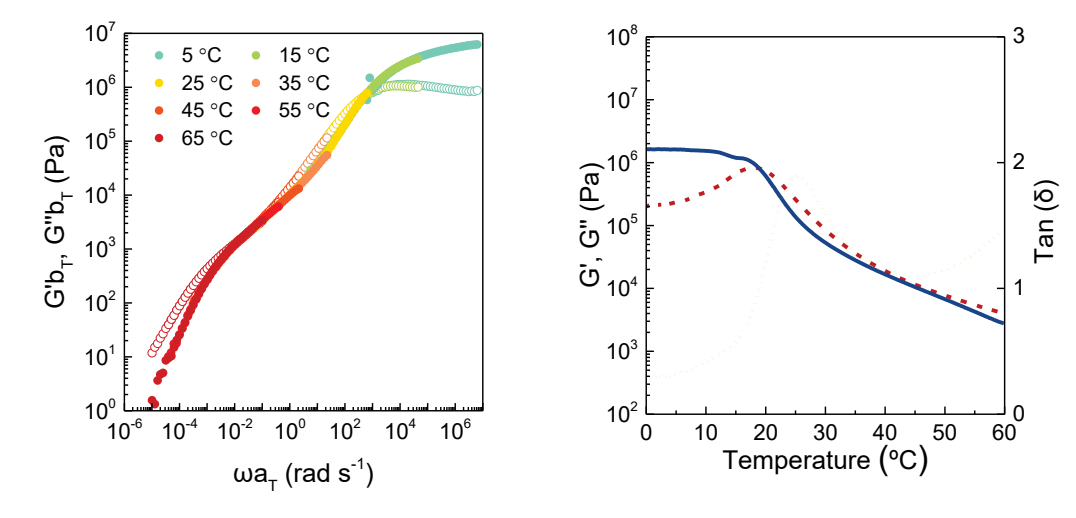


Fig. 4. Viscoelastic response for SULF4/PVBT. Left: frequency response. Right; temperature response showing a glass transition at about 25 °C, solid line G'; dashed line G"; dotted line tanδ. See Supporting Information Figure S5 for shift factors.

The UV-vis absorption and emission spectra of SULF4/PDADMA shown in Figure 5A and 5B yield insight on a possible mechanism for the jump in association enthalpy (an example of the calorimetry is shown in Figure 5C). While the UV-vis absorption spectra of SULF4 in water and in the PEC are similar, there is a strong red shift of the emission maximum in the latter, indicating excimer formation due to stacking of the planar SULF4 molecule.(47)

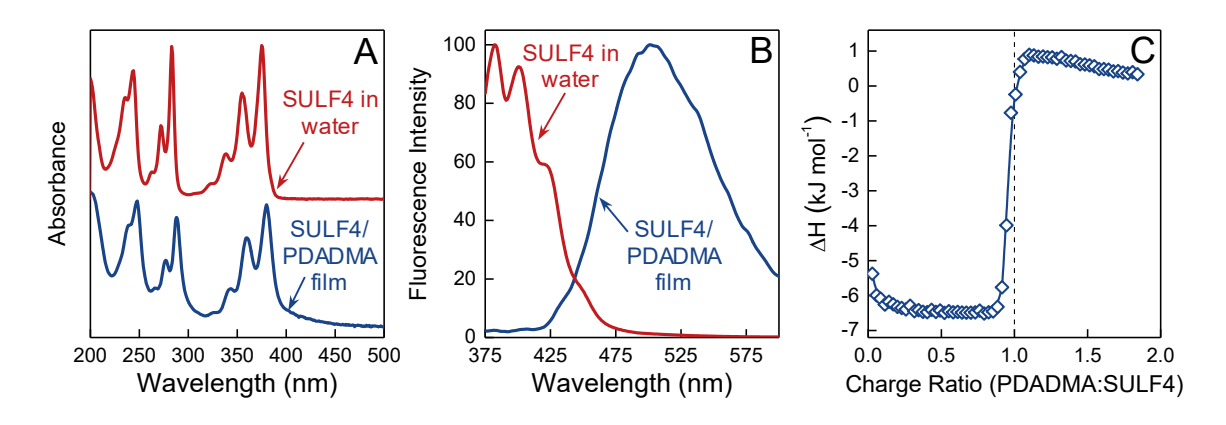


Fig. 5. Absorption, emission and calorimetry of SULF4/PDADMA A) UV-vis absorption spectra of SULF4 in water and SULF4/PDADMA film. B) fluorescence emission spectra of SULF4 in water and SULF4/PDADMA film. C) Isothermal calorimetry for the coacervation of PDADMAC (10mM) injected into SULF4 (0.25 mM) in 0.05 M NaCl at 25 °C.

15

5

10

15

20

25

30

35

Strong differences in viscoelastic properties are also illustrated in Figure 3D which compares G' for SULF3/PDADMA and SULF4/PDADMA with a solution of the chloride salt of PDADMA by itself at a similar weight% to that found in the SULF coacervates. Figure 3D also includes the VR of a coacervate between thiocyanide, SCN-, a monovalent ion on the chaotropic end of the Hofmeister series, and PDADMA (see Figure 2B for an image of this LLPS). The SCN/PDADMA coacervate contains more water (Figure 2B), and is much less viscous than its single-charged SO₃- counterpart, SULF1. It should be stressed that coacervation of the appropriate macromolecule may be induced by an ionic species carrying just one charge, drawing attention to the overlap between terminologies used to describe LLPS, including "condensation," "demixing," "precipitation," and "complexation." Such monovalent species cannot form bridges between macromolecules.

For comparison, the viscoelastic properties of a 27.5 wt% solution of PDADMA(Cl) at a concentration similar to that of the SULF series are shown in Figure 3D. This experiment was intended to show that the dynamics are slowed much more when SULF is used to prepare coacervates of the polymer having similar weight%. Though experiments are performed without added salt, the viscosities of all coacervates are expected to decrease were NaCl to be added.(13, 48)

The shape of the viscoelastic response in Figure 3D is characteristic of an entangled polymer.(49) Interestingly, the rubbery plateau modulus, recorded as the minimum of $\tan\delta$ (see Supporting Information Figure S3), remained approximately constant for the entire SULF series at about 3 x 10^4 Pa (Table 2), which is expected if the volume fractions of polymer are comparable. Because the coacervates are stoichiometric, the SO_3^- density and the density of $SO_3^-/DADMA^+$ charge pairs also remained roughly constant. The characteristic relaxation rates in Figure 3D, indicated by the crossings of G' and G", include the reptation rate, ω_{rep} , entanglement relaxation rate, ω_e , and, at the highest frequencies, the relaxation rate between the minimum number of monomer units, ω_m , visible only for SULF4 ($\sim 10^5$ s⁻¹).(10)

Valence Formation Threshold and Modulus Jump with Inorganic Phosphates

Aromatic interactions in the SULF/PDADMA series may provide additional hydrophobic or π - π bonding to help assemble coacervates. To provide a completely different, aromatic-free system, we made a more biologically relevant series of coacervates using inorganic phosphates (PHOS) and polyarginine (PARG) (Figure 6). These systems are comparable to those employing nucleoside phosphates, such as ATP, ADP or AMP, and cationic polypeptides (29) or synthetic polycations.(33) We prepared coacervates at physiological NaCl concentrations and recorded the VR. Figure 6C shows there is a strong increase in modulus from PHOS3 to PHOS4, with a minor increase to PHOS5.

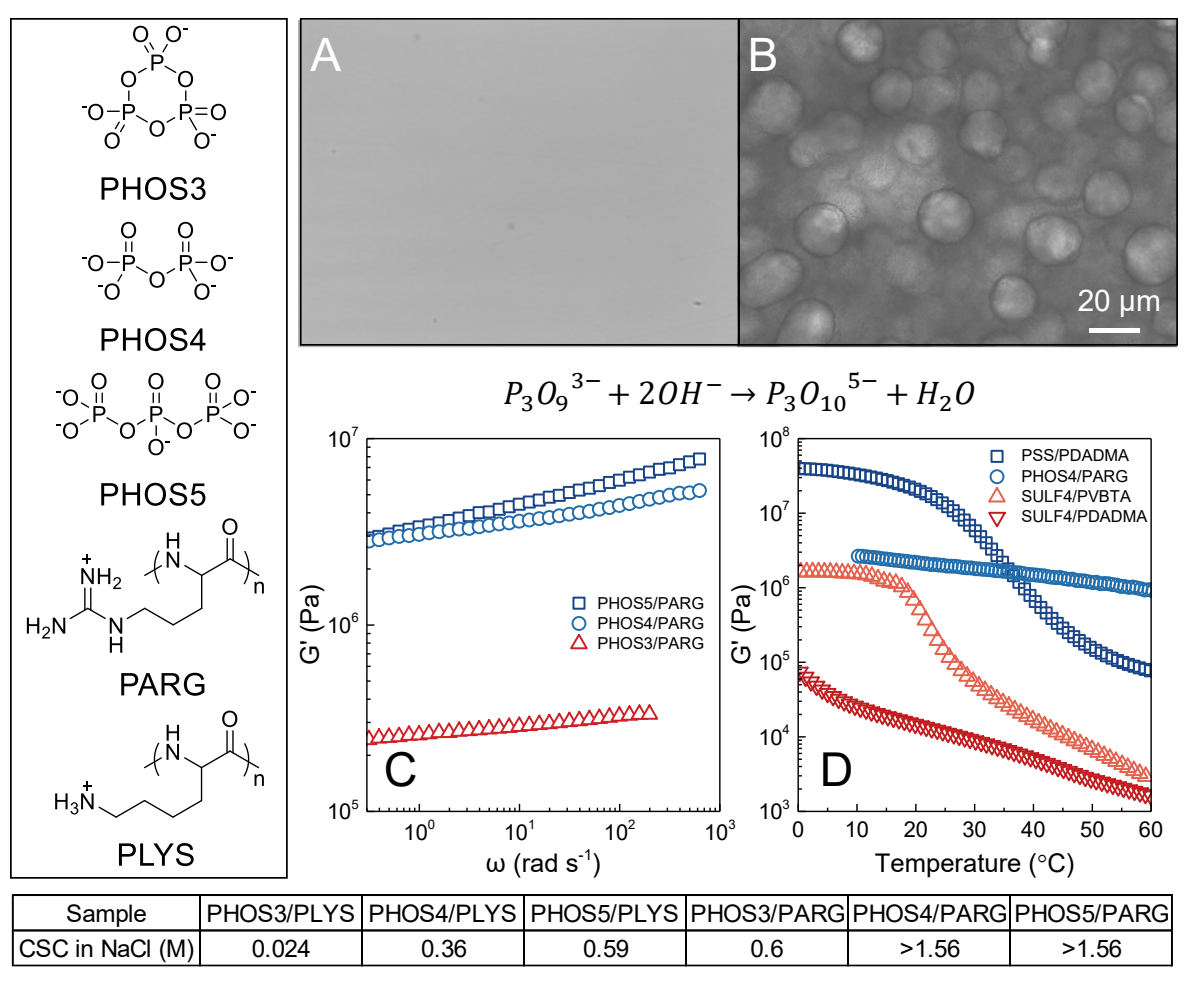


Fig. 6. Micrographs and viscoelasticity of PHOS PECs. A) Micrographs of a fresh mixture of polylysine, PLYS, and PHOS3 in 0.15 M NaCl pH 7 and (B) 12 hours after adding NaOH to hydrolyze the PHOS3 to PHOS5. C) G' *versus* frequency for PHOS/PARG coacervates at 37 °C in 0.15 M NaCl, pH = 7. See Figure S6 for G" and tanδ. D) G' *versus* temperature PSS/PDADMA, SULF4/PDADMA, SULF4/PVBTA and PHOS4/PARG in 0.01 M NaCl at 0.1 Hz. Ramp rate = 1 °C min⁻¹ for PSS/PDADMA, SULF4/PDADMA and SULF4/PVBTA, ramp rate = 2 °C min⁻¹ for PHOS4/PARG. Table at the bottom summarizes the critical salt concentration of PHOS3/PLYS, PHOS4/PLYS, PHOS5/PLYS, PHOS3/PARG, PHOS4/PARG and PHOS5/PARG in NaCl.

10

15

20

This system again exhibits a step in VR properties going from 3 to 4 charges. The accessibility of the charges on PHOS is not a limitation here. Using ChemDraw 20, we estimated the volume and solvent accessible area of PHOS3 to be 112 Å³ and 304 Å², respectively, while those of PHOS4 were 85 Å³ and 263 Å². Thus, ARG or LYS repeat units should be able to engage the charges on PHOS3.

To demonstrate the importance of the functional group in determining coacervation, no LLPS resulted when mixing polylysine instead of PARG with PHOS3. Base-induced hydrolysis (ring opening) of PHOS3 to PHOS5 yielded coacervate droplets from this mixture (Figure 6B). PHOS5/PLYS coacervation under the conditions used (pH = 7, 0.15 M NaCl) is triggered by an increase in valency of the inorganic phosphate from three to five, which increases the CSC from 0.044 M to 0.64 M (Figure 6 compares CSCs for the PHOS series).

The VR of polymers with "sticky" interactions is known to be controlled by the lifetime of these interactions- i.e. charge pairs in the present case.(50) The fastest relaxation rate (using the classical terminology of polymer physics (49)), from the smallest group of paired charges,(10) is given by ω_m , which was only observed for SULF4/PDADMA (Figure 3D). A lower ω_m shifts all characteristic relaxation rates to lower frequencies.(50) This direct connection between charge pair lifetimes and macromolecule dynamics: leads to higher viscosities and moduli. PARG forms more strongly-associating charge pairs (implying longer lifetimes), illustrated by a higher CSC (see Table in Figure 6) with PHOS than does PLYS, imparting greater viscosity and modulus to the coacervate (Figure S7 Supporting Information for a comparison of PHOS5/PARG and PHOS5/PLY).

Possible Mechanism for Jump in Modulus

5

10

15

20

25

30

35

40

45

The mechanism for the jump in coacervate VR induced by a small molecule valency change from 3 to 4 is of great interest. Multivalency influences relaxation rate to some extent. For comparison, the VR of a polymeric sulfonate, PSS, coacervated with PDADMA is also shown in Figure 6D and S8. The VR of this and other combinations of synthetic polyelectrolytes have been intensely studied. Extensive, random charge pairing between two macromolecules results in LLPS and liquid-like or solid-like materials. (10, 11, 13, 51) In a couple of examples, the actual rate of charge unpairing (the inverse of pair lifetime) has been inferred from ion conductivity measurements. (10, 52)

The jump in modulus for the SULF3 to SULF4 is clearly seen in Figure 3 by a shift of VR to lower frequencies. Both ω_r (Table 2) and the terminal region of G' (inset of Fig. 3D) shift by a factor of about 300, all other parameters remaining equal (e.g. volume fraction of polymer, length of polymer chain). A small ion with three charges can engage one polymer chain with two charge pairs and another with one charge pair. Chain relaxation is thus as fast as the breaking of the "weak link" - a single pair of charges. Four-valent ions may bridge two polymer chains with two charge pairs on each. Chain relaxation now relies on breaking two charge pairs *simultaneously*, which is much less likely and much slower.(10) Therefore, all chain dynamics are slowed and the viscosity increases substantially.

To estimate the change in the number of interactions involved at ω_r , we replotted the highest temperature points from the frequency shift data for SULF3- and SULF4/PDADMA (Figure S3) as an Arrhenius plot in Figure S9. At sufficiently high temperatures, polymer dynamics are known to exhibit Arrhenius behavior(10, 49). The activation energy for SULF3/PDADMA was 57 kJ mol⁻¹ (about the same as those for SULF1 & SULF2/PDADMA) whereas that for SULF4/PDADMA was 99 kJ mol⁻¹ – almost twice as much, consistent with a doubling of the SULF-PDADMA interactions at ω_r limiting dynamics.

Physical and Biological Relevance

Bungenberg de Jong initially thought coacervates were aggregates of colloidal particles. (1) Two decades later, he distanced himself from this view and took the modern perspective that coacervates are homogeneous phases. (2) His categorization of coacervates as "simple," relying on nonionized groups for interaction, and "complex," which are driven by charges and the formation of "salt bonds" (charge pairs), was probably too basic for biomolecule coacervation, but adequate for synthetic systems which can be designed with less complexity. Interestingly, he relied heavily on hexol, (2) $\text{Co}[(\mu\text{-OH})_2\text{Co}(\text{NH}_3)_4]_3(\text{NO}_3)_6$, a hexavalent cobalt complex first made by Jorgensen, (53) and later studied by Werner, (54) to coacervate acidic proteins. As seen in Figure 2, coacervation of a synthetic polyelectrolyte relying on charge needs only a single-charged

hydrophobic ion to induce phase separation. The "strength" of coacervation, reported by the CSC, cannot be judged solely by the amount of water expelled or the "hydrophobicity" of the coacervating components (compare the coacervate volumes and CSC in Table 1). Cooperativity of charge pairing also plays a major role in the CSC. This cooperativity is not reflected in the viscoelasticity until four charges are involved. In a recent mechanism for polymer/polymer coacervates we concluded the minimum cooperatively rearranging unit in PEC dynamics was an exchange of two Pol⁺Pol⁻ pairs with a relaxation rate for PDADMA/PSS of about $10^4 \, \mathrm{s}^{-1}$.(55) A ω_m of about $10^5 \, \mathrm{s}^{-1}$ in Figure 3D is consistent with pair exchange in a material similar to PDADMA/PSS containing more water.

Biological structures also exhibit a significant range of viscoelastic response. The loss of dynamics and physical reversibility at the molecular level may lead to larger-scale aggregation and morphology variations in organs and organelles. Aggregation may be induced by functionality transformation (e.g. lysine to arginine); change of charge density (e.g. (de)phosphorylation); misfolding (allowing two strongly interacting groups, that would normally be held apart, to approach); a change of registry/sequence of opposite charges; or similar changes in chaperones that facilitate *disassembly*.(56) The significant finding in our work is that a sudden increase in local cooperativity, leading to a strong increase in solid-like character, occurs with a transition from 3 to 4 nearby charge pairs. This mechanism is in addition to the slow aging of tissues from the loss of (plasticizing) water, greater crosslinking and other aging mechanisms.

MATERIALS AND METHODS

Materials

5

10

15

20

25

30

35

40

45

2-naphthalenesulfonic acid, sodium salt (SULF1, 90%), 1,5-naphthalenedisulfonic acid, disodium salt (SULF2, 95%), 1,3,6-naphthalenetrisulfonic acid, trisodium salt hydrate (SULF3), and 1,3,6,8-pyrenetetrasulfonic acid, tetrasodium salt hydrate (SULF4, 98%) were from Sigma-Aldrich. Trisodium trimetaphosphate (PHOS3, 95%), sodium pyrophosphate tetrabasic (PHOS4, 95%), and sodium triphosphate pentabasic (PHOS5, 98%) were from Sigma-Aldrich. Sodium thiocyanate (NaSCN) was from VWR. Medium molecular weight poly(diallyldimethylammonium chloride) (PDADMAC, 20 wt% in water, molecular weight, MW, 200,000-350,000) was from Aldrich. Poly-*L*-arginine hydrochloride (PARG, MW = 38,500) and poly-*L*-lysine hydrochloride (PLYS, MW = 66,000) were from Alamanda Polymers. Poly(vinylbenzyl trimethylammonium chloride) (PVBTAC, 27 wt% in water, MW 100,000) was from Scientific Polymer Products. 18 MΩ cm deionized water (Barnstead, Nanopure) was used to prepare all solutions.

PDADMAC Fractionation

Commercial samples of PDADMAC usually have broad molecular weight distributions, MWD, M_w/M_n . PDADMAC specified to be in the MW range 200,000-350,000 by Sigma-Aldrich was fractionated to narrow the MWD of PDADMAC from 3.3 to 1.4 As-received PDADMAC solution was diluted to 10 wt% in water. Acetone (99.5%, VWR) was gradually added into 100 mL 10 wt% PDADMAC solution until the solution became cloudy. Then the cloudy solution was centrifuged at 6000 rpm until the supernate became transparent. The supernate was collected and the same fractionation procedure was repeated two more times to remove most of the high molecular weight PDADMAC. Finally, the third fraction of PDADMAC was collected and dried at 120 °C for 24 h.

Size Exclusion Chromatography

The weight average molecular weight, M_w , number average molecular weight M_n , and MWD of PDADMAC before and after fractionation were determined by size exclusion chromatography with light scattering detection. 50 μL of 2 mg mL⁻¹ PDADMAC in 0.3 M NaNO₃

was injected through a 300 mm \times 8 mm, PSS Inc. Novema Max Lux 1000 Å analytical column guarded by a 10 μ m Novema Max Lux guard column. 0.3 M NaNO₃ preserved with 200 ppm NaN₃ was used as the mobile phase. A DAWN-EOS multiangle light scattering detector in series with a rEX refractometer (Wyatt Technology) were used to collect molecular weight data. The refractive index increment, dn/dc, for PDADMAC in 0.3 M NaNO₃ was 0.186, which was measured with the refractometer using an offline mode. Figure S1 shows the chromatograms.

Sulfonate/PDADMA Coacervates

SULF1, SULF2, SULF3 and SULF4 were dried under vacuum at 120 °C for 24 h. 10 mL 0.3 M PDADMAC (fractionated) solution was mixed with 10 mL 0.3 M SULF1, 0.15 M SULF2, 0.1 M SULF3 and 0.075 M SULF4 to form SULF1/PDADMA, SULF2/PDADMA, SULF3/PDADMA and SULF4/PDADMA coacervates, respectively. The mixtures were centrifuged at 6000 rpm for 24 h to collect the coacervates.

SULF4/PDADMA Film

5

10

15

20

25

30

35

40

45

Bulk SULF4/PDADMA coacervates were too absorbing to study by UV-vis transmission spectroscopy. Therefore, SULF4/PDADMA films were built on fused silica using a robot (Stratosequence V, NanoStrata Inc.) to perform a layer-by-layer assembly. A "bilayer" was made by dipping the quartz in 1 mM PDADMAC solution for 5 min, followed by 5 min dipping in 10 mM SULF4. After 15 bilayers of SULF4/PDADMA film were deposited, the silica was removed, and films were dried under a stream N₂.

Phosphate-polypeptide Coacervates

Poly-*L*-arginine, poly-*L*-lysine, and phosphate salts were vacuum dried at room temperature for 24 h before transfer to an argon filled glove box to be weighed. 0.125 M poly-*L*-arginine and poly-*L*-lysine solutions in 0.15 M NaCl, 20 mM 3-(N-morpholino)propanesulfonic acid (MOPS) buffer, and 200 ppm sodium azide were mixed with equal volumes of phosphate salt solutions at molar concentrations resulting in stoichiometric charge ratios. The resulting coacervates were then vortexed for 10 min and centrifuged for 4 h at 12,000 rpm. The supernate was removed from the centrifuge tube and coacervates were partially dried under vacuum for 6 h. The coacervates were placed into a stainless steel 8 mm diameter mold and pressed at room temperature for 24 h. The polyelectrolyte coacervate tablets were then removed from the mold and placed into a 20 mL vial filled with a solution at 0.15 M NaCl, 20 mM MOPS pH 7, and 200 ppm sodium azide to equilibrate for 24 h.

NMR Spectroscopy

The stoichiometries of SULF/PDADMA coacervates were determined using solution ¹H NMR spectroscopy. NMR samples were prepared by dissolving the dry PEC in a solution of KBr in D₂O. This allowed the number of protons on both the small molecules and polyelectrolytes to be measured. The KBr concentrations used in NMR sample preparation were different from one to another since the CSCs required to fully dissociate the PECs were different. For SULF1/PDADMA, SULF2/PDADMA and SULF3/PDADMA, 10 mg of the dry PEC was dissolved in 1.0 M KBr in D₂O, whereas 10 mg of dry SULF4/PDADMA was dissolved in 3.0 M KBr in D₂O. An AVANCE 600 MHz NMR (Bruker) was used to acquire the spectra. NMR spectra are shown in Figure S2.

UV-Vis Spectroscopy

UV-vis absorption spectra were obtained on a UV 2450 absorption spectrophotometer (Shimadzu). The quartz slide bearing the SULF4/PDADMA film was mounted on a custom-designed sample holder. The absorption of 10^{-5} M SULF4 in water was also measured in a fused silica cuvette.

Emission spectroscopy

SULF4/PDADMA film fluorescence emission spectra were recorded on a Horiba Fluoromax-4 spectrofluorometer. Samples were excited at 370 nm and emission was measured from 375 to 600 nm. Emission intensity was recorded every 1 nm, excitation and emission slit widths were 1 nm, and the integration time was 0.5 s.

Critical Salt Concentration (CSC)

5

10

15

20

25

30

35

40

45

The CSCs of SULF/PDADMA coacervates were determined with the gradual addition of NaCl to a 1 mg mL⁻¹ suspension of PEC particles, prepared by mixing salt-free solutions of PEC components. The CSC was taken to be [NaCl] at which solutions became clear (visibly and by turbidimetry). The CSCs of PHOS/PARG and PHOS/PLYS PECs were also determined using this method. In the case of PHOS4/PARG and PHOS5/PARG it was found that the PECs were insoluble up to 6M NaCl and therefore the CSC is unknown.

Isothermal Titration Calorimetry (ITC)

PDADMAC was dialyzed (3,500 molecular weight cutoff tubing, SnakeSkin, ThermoFisher) against deionized water for 2 days, with water replacement every 12 h. The PDADMAC solution was then freeze-dried (Labcono, FreeZone 105) to a powder. The sulfonate salts (SULF1, SULF2, SULF3, SULF4) and PDADMAC powder were dried at 110 °C for 4 h, then immediately moved into an argon filled glovebox to be weighed.

ITC was performed using a VP-ITC (MicroCal Inc.) calorimeter. The ITC was calibrated with an internal y-axis calibration followed by a standard titration between hydrochloric acid and Tris base. All samples were degassed for 10 min at room temperature. Approximately 300 μL of a 10 mM PDADMAC solution were loaded into the syringe. 10 μL of the PDADMAC solution were manually discharged from the syringe to relieve any back pressure from the loading process. Prior to filling, the sample cell (1.4138 mL) was washed with the SULF solution. To accommodate the amount of charge on one molecule and the limited number of injections that are allowed, the trivalent SULF3 and quadrivalent SULF4 salts were 0.25 mM solutions while the monovalent and divalent salts were 0.5 mM solutions. The syringe was rotated at 260 rpm in the sample cell with an injection size of 4 μL per aliquot at a rate of 0.50 μL s $^{-1}$, with 240 s between injections. The heat flow was recorded as a function of time at 25.0 °C. Enthalpies were calculated by summing the total heat generated to the end point with a correction for the background dilution enthalpy (see Supporting Information Figure S10 for ITC thermograms). The dilution enthalpy was determined from the addition of 10 mM PDADMAC into water under identical conditions.

Viscoelastic Response, VR

Measurements of linear viscoelastic responses were performed using a stress-controlled DHR-3 rheometer (TA Instruments) with Peltier temperature control. A 20 mm parallel plate was used for all experiments except for polypeptide-PHOS coacervate, where an 8 mm parallel plate was used. A custom-designed lower plate in a solution reservoir with a cap was used to prevent evaporation. The coacervates were first transferred onto the lower plate. The upper plate was then lowered onto the samples to provide a ~100 μm gap. The excess coacervate was trimmed off and the desired aqueous solution was added to the solution reservoir to maintain the environment for coacervates. Frequency sweep experiments were performed on the samples at temperatures ranging from -5 °C to 65 °C. 15 min was allowed for samples to reach temperature equilibrium. Temperature ramp experiments were carried out at 1 Hz with a ramp rate of 1 °C min⁻¹. Strain sweep experiments were performed from 0.01 to 100% strain to ensure all responses were within the linear viscoelastic regime.

PHOS/PLYS Coacervate Hydrolysis

A 0.5 mL solution (pH 7, 0.15 M NaCl, 200 ppm sodium azide, 20 mM MOPS) with 0.15 M polylysine was mixed with 0.5 mL of a 0.05 M PHOS3 solution (identical pH, salts, and buffer).

No coacervation was observed. The solution was vortexed for 5 min and the pH was increased to 9 by adding concentrated NaOH. The solution was then placed in a tissue culture plate and moved to the imaging stage of a Nikon Eclipse Ti-DH Inverted Microscope equipped with a Photometrics Coolsnap HQ2 CCD camera (1392×1040 , $6.45 \, \mu m^2$ pixels). The culture plate was left on the imaging stage for 12 h without movement, while images were taken periodically.

References and Notes

5

10

15

25

30

35

40

- 1. H. G. Bungenberg de Jong, H. R. Kruyt, Coacervation (partial miscibility in colloid systems). *Proc. Sect. Sci. K. Ned. Akad. Wetenschappen* **32**, 849-856 (1929).
- 2. H. G. Bungenberg de Jong, in *Colloid Science,* H. R. Kruyt, Ed. (Elsevier, Amsterdam, 1949), vol. 2, chap. Chapters 7,8.9,10 and 11.
- 3. A. A. Hyman, C. A. Weber, F. Jülicher, Liquid-Liquid Phase Separation in Biology. *Annual Review of Cell and Developmental Biology* **30**, 39-58 (2014).
- 4. C. D. Keating, Aqueous Phase Separation as a Possible Route to Compartmentalization of Biological Molecules. *Accounts of Chemical Research* **45**, 2114-2124 (2012).
- 5. Y. Lin, David S. W. Protter, Michael K. Rosen, R. Parker, Formation and Maturation of Phase-Separated Liquid Droplets by RNA-Binding Proteins. *Mol Cell* **60**, 208-219 (2015).
- 6. A. Borgia *et al.*, Extreme disorder in an ultrahigh-affinity protein complex. *Nature* **555**, 61-66 (2018).
- 7. D. L. J. Lafontaine, J. A. Riback, R. Bascetin, C. P. Brangwynne, The nucleolus as a multiphase liquid condensate. *Nat Rev Mol Cell Bio* **22**, 165-182 (2021).
 - 8. C. P. Brangwynne, P. Tompa, R. V. Pappu, Polymer physics of intracellular phase transitions. *Nat Phys* **11**, 899-904 (2015).
 - 9. C. E. Sing, S. L. Perry, Recent progress in the science of complex coacervation. *Soft Matter* **16**, 2885-2914 (2020).
 - 10. K. Akkaoui, M. Yang, Z. A. Digby, J. B. Schlenoff, Ultraviscosity in Entangled Polyelectrolyte Complexes and Coacervates. *Macromolecules* **53**, 4234-4246 (2020).
 - 11. A. B. Marciel, S. Srivastava, M. V. Tirrell, Structure and rheology of polyelectrolyte complex coacervates. *Soft Matter* **14**, 2454-2464 (2018).
 - 12. E. Spruijt, A. H. Westphal, J. W. Borst, M. A. Cohen Stuart, J. van der Gucht, Binodal Compositions of Polyelectrolyte Complexes. *Macromolecules* **43**, 6476-6484 (2010).
 - 13. E. Spruijt, M. A. Cohen Stuart, J. van der Gucht, Linear Viscoelasticity of Polyelectrolyte Complex Coacervates. *Macromolecules* **46**, 1633-1641 (2013).
 - 14. R. Chollakup, W. Smitthipong, C. D. Eisenbach, M. Tirrell, Phase Behavior and Coacervation of Aqueous Poly(acrylic acid)-Poly(allylamine) Solutions. *Macromolecules* **43**, 2518-2528 (2010).
 - 15. A. S. Michaels, Polyelectrolyte complexes. *Journal of Industrial and Engineering Chemistry* **57**, 32-40 (1965).
 - 16. E. Tsuchida, Formation of Polyelectrolyte Complexes and Their Structures. *Journal of Macromolecular Science, Part A* **31**, 1-15 (1994).
 - 17. R. M. Fuoss, H. Sadek, Mutual interaction of polyelectrolytes. *Science* **110**, 552-554 (1949).
 - 18. B. Philipp, H. Dautzenberg, K. J. Linow, J. Kötz, W. Dawydoff, Poly-Electrolyte Complexes Recent Developments and Open Problems. *Prog Polym Sci* **14**, 91-172 (1989).
 - 19. K. Abe, H. Ohno, E. Tsuchida, Phase changes of polyion complex between poly(methacrylic acid) and a polycation carrying charges in the chain backbone. *Die Makromolekulare Chemie* **178**, 2285-2293 (1977).
 - 20. Q. F. Wang, J. B. Schlenoff, The Polyelectrolyte Complex/Coacervate Continuum. *Macromolecules* **47**, 3108-3116 (2014).

10

15

20

25

30

35

40

- 21. G. Krainer *et al.*, Reentrant liquid condensate phase of proteins is stabilized by hydrophobic and non-ionic interactions. *Nat Commun* **12**, 1085 (2021).
- 22. J. B. Schlenoff, M. Yang, Z. A. Digby, Q. Wang, Ion Content of Polyelectrolyte Complex Coacervates and the Donnan Equilibrium. *Macromolecules* **52**, 9149-9159 (2019).
- J. Huang, F. J. Morin, J. E. Laaser, Charge-Density-Dominated Phase Behavior and Viscoelasticity of Polyelectrolyte Complex Coacervates. *Macromolecules* **52**, 4957-4967 (2019).
- 24. A. Molliex *et al.*, Phase Separation by Low Complexity Domains Promotes Stress Granule Assembly and Drives Pathological Fibrillization. *Cell* **163**, 123-133 (2015).
- 25. R. S. Fisher, S. Elbaum-Garfinkle, Tunable multiphase dynamics of arginine and lysine liquid condensates. *Nat Commun* **11**, 4628 (2020).
- 26. J.-M. Choi, A. S. Holehouse, R. V. Pappu, Physical Principles Underlying the Complex Biology of Intracellular Phase Transitions. *Annual Review of Biophysics* **49**, 107-133 (2020).
- 27. P. Li *et al.*, Phase transitions in the assembly of multivalent signalling proteins. *Nature* **483**, 336-340 (2012).
- 28. E. Tsuchida, Y. Osada, The rôle of the chain length in the stability of polyion complexes. *Die Makromolekulare Chemie* **175**, 593-601 (1974).
 - 29. S. Koga, D. S. Williams, A. W. Perriman, S. Mann, Peptide–nucleotide microdroplets as a step towards a membrane-free protocell model. *Nat. Chem.* **3**, 720-724 (2011).
 - 30. F. P. Cakmak, S. Choi, M. O. Meyer, P. C. Bevilacqua, C. D. Keating, Prebiotically-relevant low polyion multivalency can improve functionality of membraneless compartments. *Nat Commun* **11**, 5949 (2020).
 - 31. W. M. Aumiller, C. D. Keating, Phosphorylation-mediated RNA/peptide complex coacervation as a model for intracellular liquid organelles. *Nat Chem* **8**, 129-137 (2016).
 - 32. W. M. Aumiller, F. P. Cakmak, B. W. Davis, C. D. Keating, RNA-Based Coacervates as a Model for Membraneless Organelles: Formation, Properties, and Interfacial Liposome Assembly. *Langmuir* **32**, 10042-10053 (2016).
 - 33. E. A. Frankel, P. C. Bevilacqua, C. D. Keating, Polyamine/Nucleotide Coacervates Provide Strong Compartmentalization of Mg2+, Nucleotides, and RNA. *Langmuir* **32**, 2041-2049 (2016).
 - 34. J. Fu, H. M. Fares, J. B. Schlenoff, Ion-Pairing Strength in Polyelectrolyte Complexes. *Macromolecules* **50**, 1066-1074 (2017).
 - 35. C. K. Trinh, W. Schnabel, Ionic-Strength Dependence of the Stability of Polyelectrolyte Complexes Its Importance for the Isolation of Multiply-Charged Polymers. *Angew Makromol Chem* **212**, 167-179 (1993).
 - 36. L. Li *et al.*, Phase Behavior and Salt Partitioning in Polyelectrolyte Complex Coacervates. *Macromolecules* **51**, 2988-2995 (2018).
 - 37. C. E. Sing, Development of the modern theory of polymeric complex coacervation. *Adv Colloid Interfac* **239**, 2-16 (2017).
 - 38. J. T. G. Overbeek, M. J. Voorn, Phase separation in polyelectrolyte solutions. Theory of complex coacervation. *Journal of Cellular and Comparative Physiology* **49**, 7-26 (1957).
 - 39. P. Zhang, K. Shen, N. M. Alsaifi, Z.-G. Wang, Salt Partitioning in Complex Coacervation of Symmetric Polyelectrolytes. *Macromolecules* **51**, 5586-5593 (2018).
 - 40. C. Mathieu, R. V. Pappu, J. P. Taylor, Beyond aggregation: Pathological phase transitions in neurodegenerative disease. *Science* **370**, 56-60 (2020).
 - 41. J. Wang *et al.*, A Molecular Grammar Governing the Driving Forces for Phase Separation of Prion-like RNA Binding Proteins. *Cell* **174**, 688-699.e616 (2018).
 - 42. S. Boyko, X. Qi, T.-H. Chen, K. Surewicz, W. K. Surewicz, Liquid-liquid phase separation of tau protein: The crucial role of electrostatic interactions. *J Biol Chem* **294**, 11054-11059 (2019).

- 43. S. Boeynaems *et al.*, Spontaneous driving forces give rise to protein–RNA condensates with coexisting phases and complex material properties. *Proceedings of the National Academy of Sciences* **116**, 7889-7898 (2019).
- 44. L. Jawerth et al., Protein condensates as aging Maxwell fluids. Science 370, 1317-1323 (2020).
- 45. M. Yang, Z. A. Digby, J. B. Schlenoff, Precision Doping of Polyelectrolyte Complexes: Insight on the Role of Ions. *Macromolecules* **53**, 5465-5474 (2020).
- 46. R. G. Larson, Y. Liu, H. Li, Linear viscoelasticity and time-temperature-salt and other superpositions in polyelectrolyte coacervates. *Journal of Rheology* **65**, 77-102 (2021).
- 47. F. Caruso, E. Donath, H. Möhwald, R. Georgieva, Fluorescence studies of the binding of anionic derivatives of pyrene and fluorescein to cationic polyelectrolytes in aqueous solution.

 Macromolecules 31, 7365-7377 (1998).
- 48. R. F. Shamoun, H. H. Hariri, R. A. Ghostine, J. B. Schlenoff, Thermal Transformations in Extruded Saloplastic Polyelectrolyte Complexes. *Macromolecules* **45**, 9759-9767 (2012).
- 49. M. Rubinstein, R. H. Colby, *Polymer Physics*. (Oxford University Press, New York, 2003).
- 50. M. Rubinstein, A. N. Semenov, Dynamics of Entangled Solutions of Associating Polymers. *Macromolecules* **34**, 1058-1068 (2001).
 - 51. S. Manoj Lalwani, C. I. Eneh, J. L. Lutkenhaus, Emerging trends in the dynamics of polyelectrolyte complexes. *Physical Chemistry Chemical Physics* **22**, 24157-24177 (2020).
 - 52. S. A. Shaheen, M. Yang, B. Chen, J. B. Schlenoff, Water and Ion Transport through the Glass Transition in Polyelectrolyte Complexes. *Chemistry of Materials* **32**, 5994-6002 (2020).
 - 53. S. M. Jörgensen, Zur Konstitution der Kobalt-, Chrom- und Rhodiumbasen. X. Mitteilung. *Zeitschrift für anorganische Chemie* **16**, 184-197 (1898).
 - 54. A. Werner, Über mehrkernige Metallammoniake. *Berichte der deutschen chemischen Gesellschaft* **40**, 4434-4441 (1907).
- J. B. Schlenoff, K. Akkaoui, Dissecting Dynamics Near the Glass Transition Using Polyelectrolyte Complexes. *Macromolecules* **54**, 3413-3422 (2021).
 - 56. J. A. Riback *et al.*, Stress-Triggered Phase Separation Is an Adaptive, Evolutionarily Tuned Response. *Cell* **168**, 1028-1040.e1019 (2017).
 - **Acknowledgements:** The authors are grateful to the Nuclear Magnetic Resonance Laboratory Core Facility, RRID:SCR 017380 for help with NMR and to the Physical Biochemistry Core Facility, RRID:SCR 016714 for access to ITC.
- Funding: This work was supported by a grant from National Science Foundation (DMR-1809304 and DMR-2103704)
 - **Author contributions:** M.Y., Z.A.D and Y.C. performed experimental work. J.B.S. directed and coordinated research. All authors prepared the manuscript.
 - **Competing interests:** Authors declare that they have no competing interests.
 - **Data and materials availability:** All data are available in the manuscript or the supplementary materials.
 - **Supplementary Materials**

Figs. S1 to S10

5

10

15

20

30

40

Supplementary Materials for

Valence-Induced Jumps in Coacervate Properties

Mo Yang, Zachary A. Digby, Yuhui Chen, Joseph B. Schlenoff*

Correspondence to: jschlenoff@fsu.edu

This PDF file includes:

Figs. S1 to S10

5

10

15

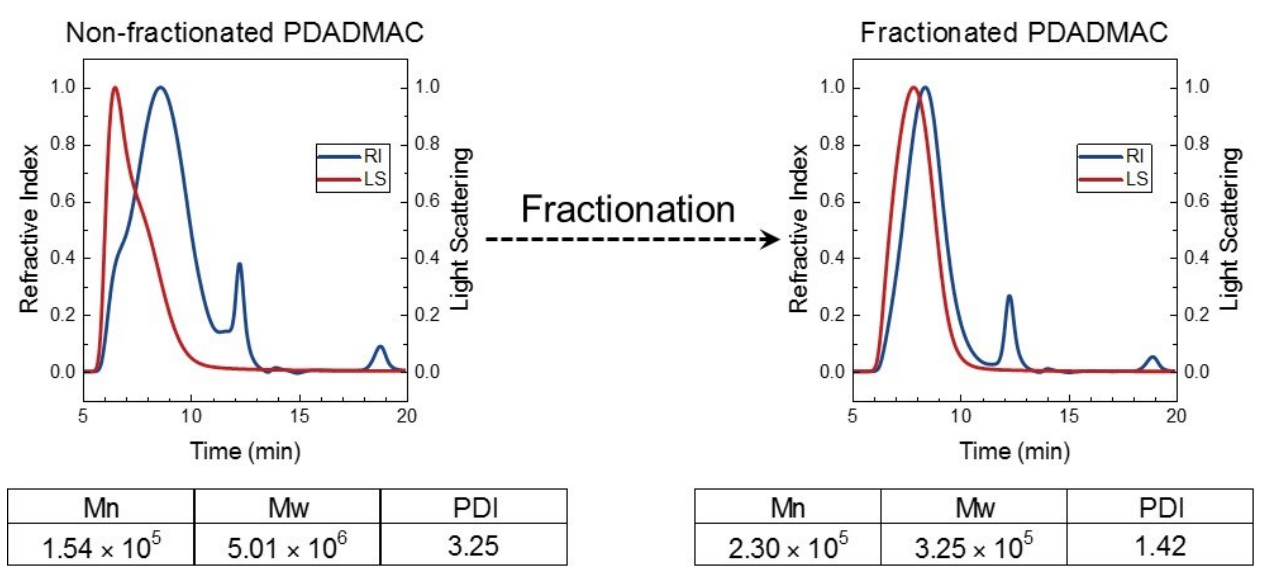


Fig. S1. SEC chromatograms of as-received "medium" molecular weight PDADMAC and fractioned PDADMAC used in this study. Number average molecular weight, M_n , weight average molecular weight, M_w , polydispersity index (PDI = M_w/M_n).

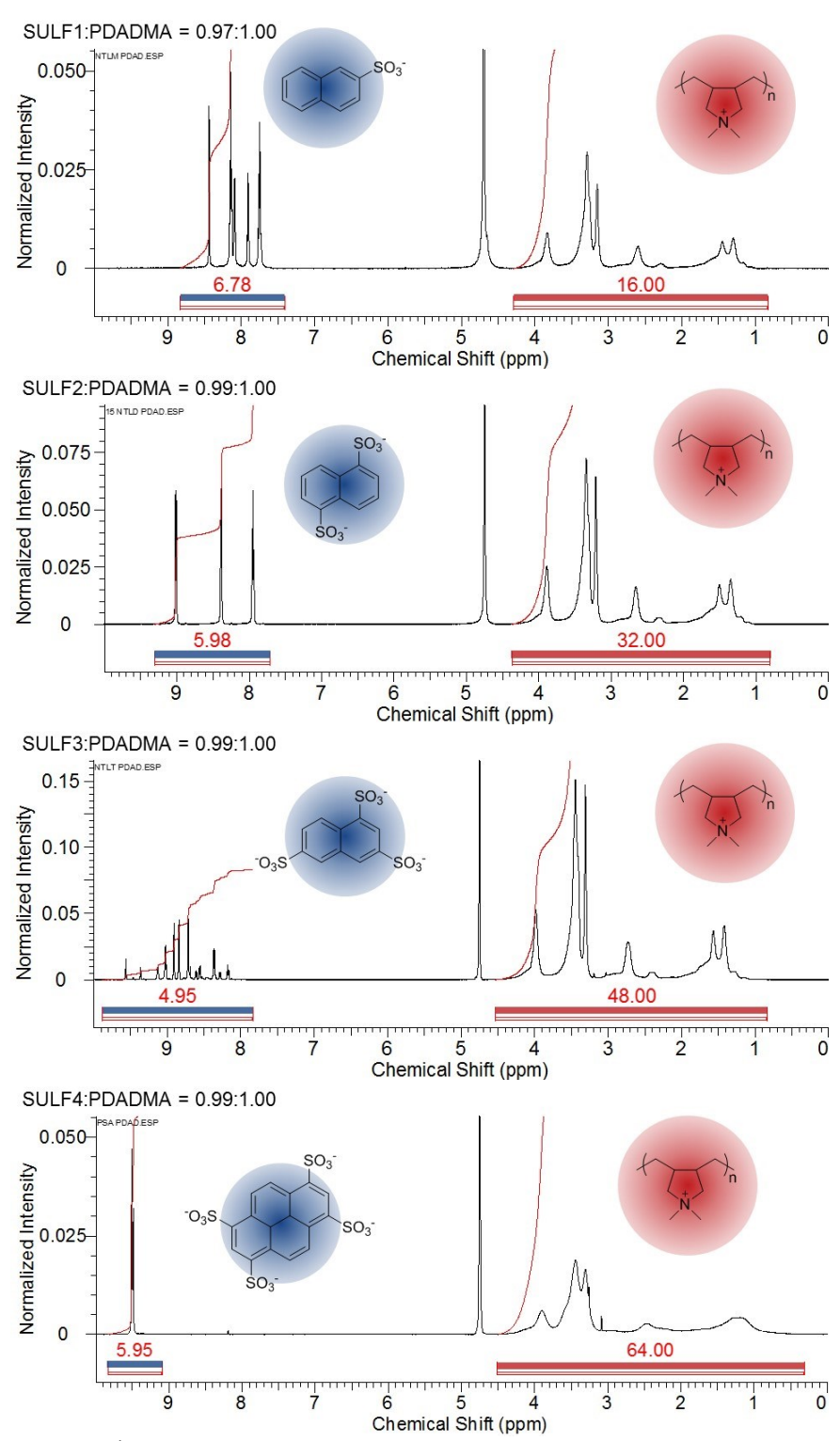


Fig. S2. ¹H NMR spectra of SULF1/PDADMA, SULF2/PDADMA, SULF3/PDADMA and SULF4/PDADMA coacervate dissolved in KBr in D₂O solution at room temperature. Aromatic ¹H >6 ppm. Aliphatic ¹H <5 ppm. Integrated peak areas for these regions are shown.

Time-temperature superposition was achieved using the two equations below:

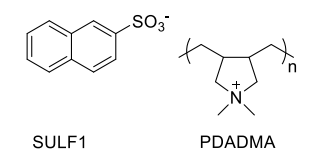
5

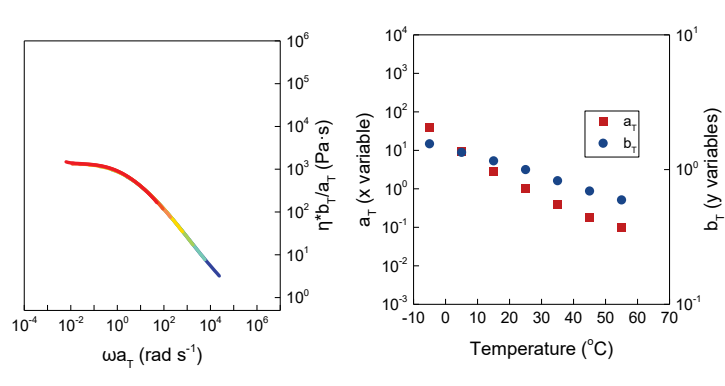
$$G'(\omega,T) = G'(a_T\omega,T_o)/b_T$$

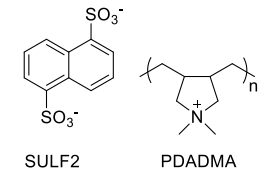
$$G''(\omega,T) = G''(a_T\omega,T_o)/b_T$$

Where ω is frequency, T is experimental temperature, a_T is the x-axis shift factor and b_T is the y-axis shift factor. T_0 is reference temperature, which was 25 °C.

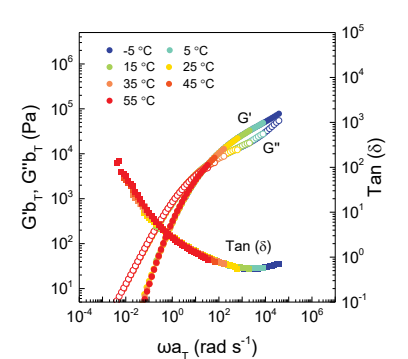
10



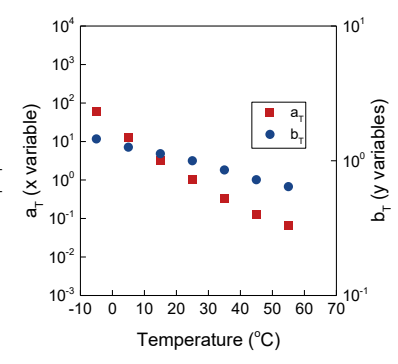


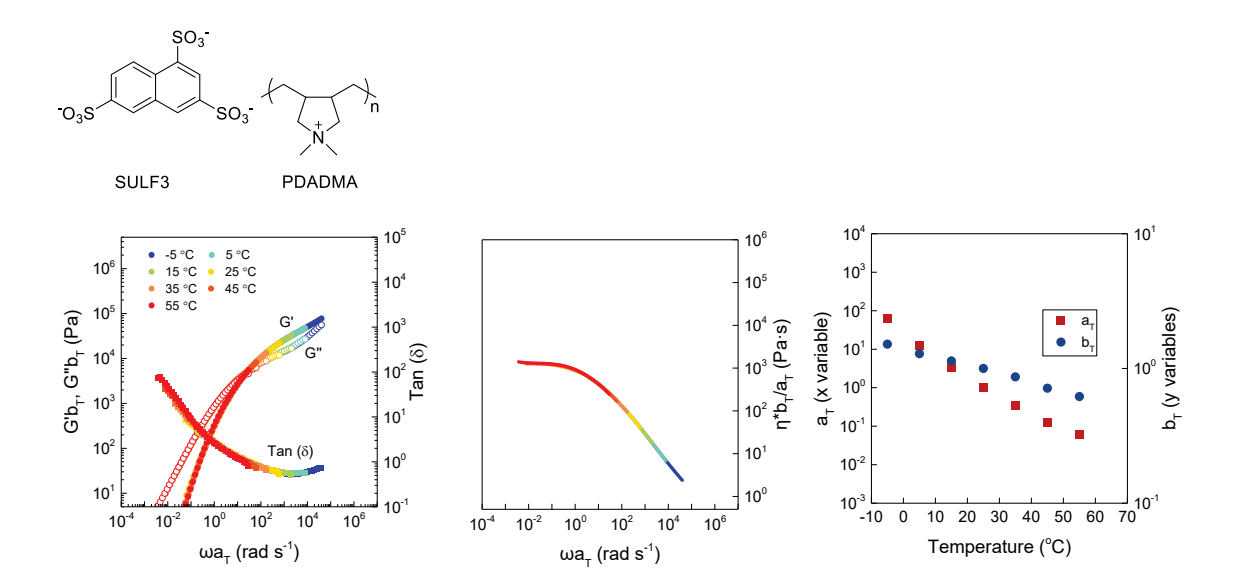


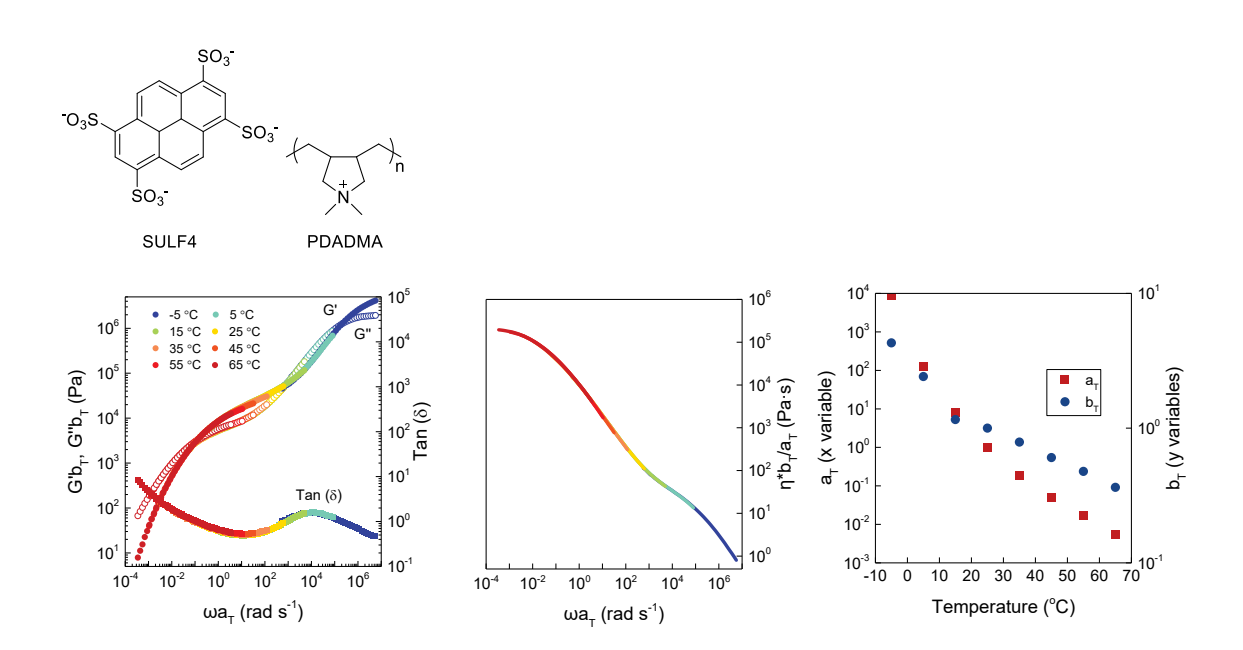
15



10⁶







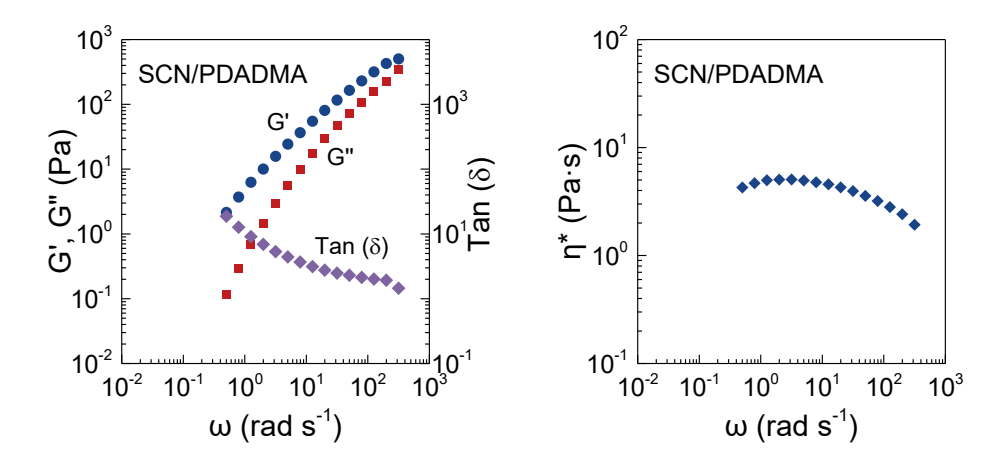


Fig. S3. Time-temperature superposition of SULF1/PDADMA, SULF2/PDADMA, SULF3/PDADMA, SULF4/PDADMA, and SCN/PDADMA coacervates in 0.01 M NaCl. G' and G" on the left panels, complex viscosity on the middle panel. Plateau values in viscosity at low frequencies were recorded as zero-shear viscosity. Reference temperature is 25 °C. Frequency responses recorded at different temperatures were shifted along the frequency axis using the shift factor a_T on the right-hand panels

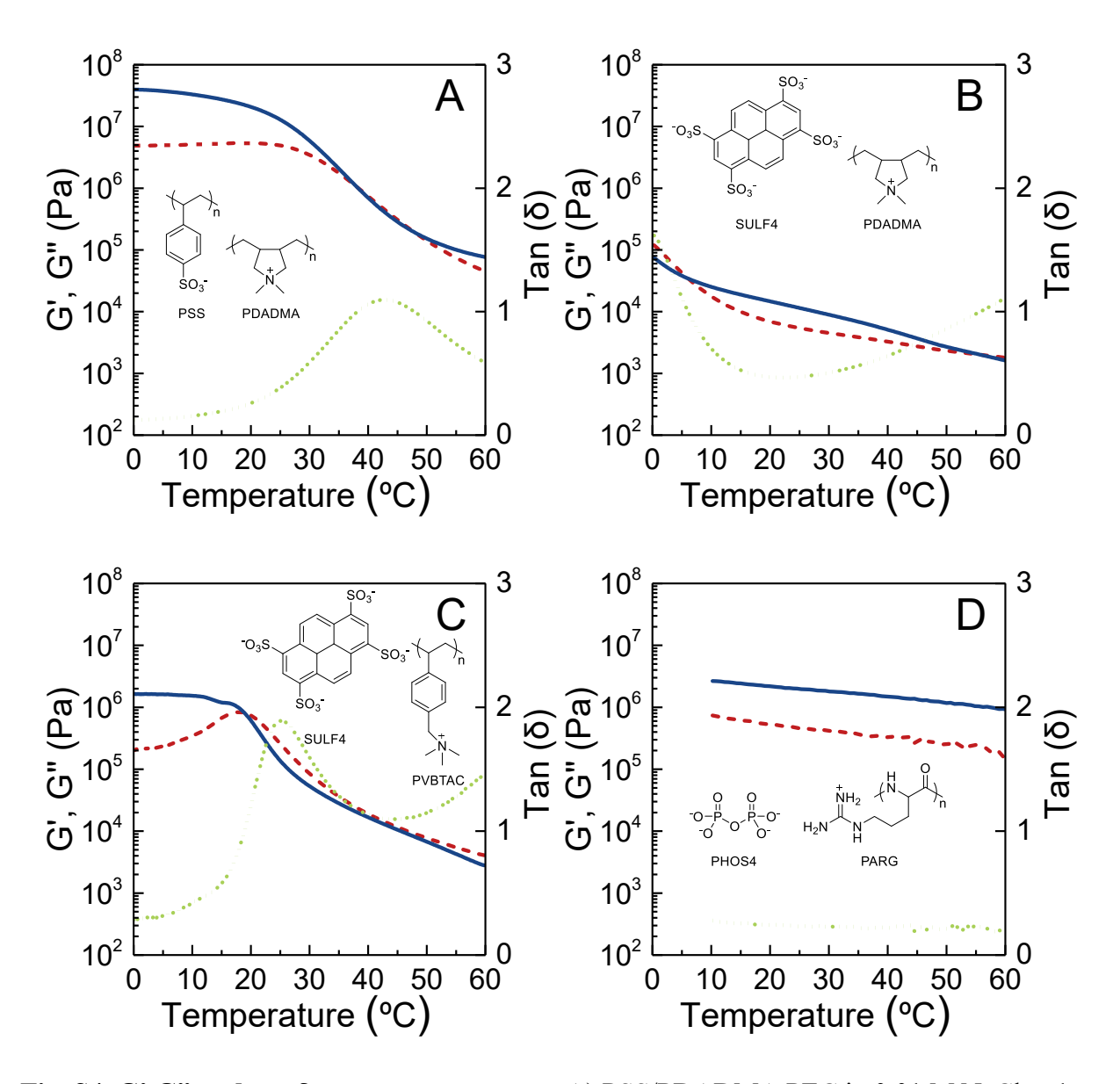


Fig. S4. G' G" and tan δ versus temperature. A) PSS/PDADMA PEC in 0.01 M NaCl at 1 Hz; B) SULF4/PDADMA in 0.01 M NaCl at 1 Hz; C) SULF4/PVBTA in 0.01 M NaCl at 1 Hz and D) PHOS4/PARG in 0.01 M NaCl at 0.1 Hz. Ramp rate = 1 °C min⁻¹ for PSS/PDADMA, SULF4/PDADMA and SULF4/PVBTA, ramp rate = 2 °C min⁻¹ for PHOS4/PARG. The peak in tan δ corresponds to a glass transition between glassy (lower temperatures) to rubbery (higher temperatures). Solid line, G'; dashed line, G"; dotted line, tan δ.

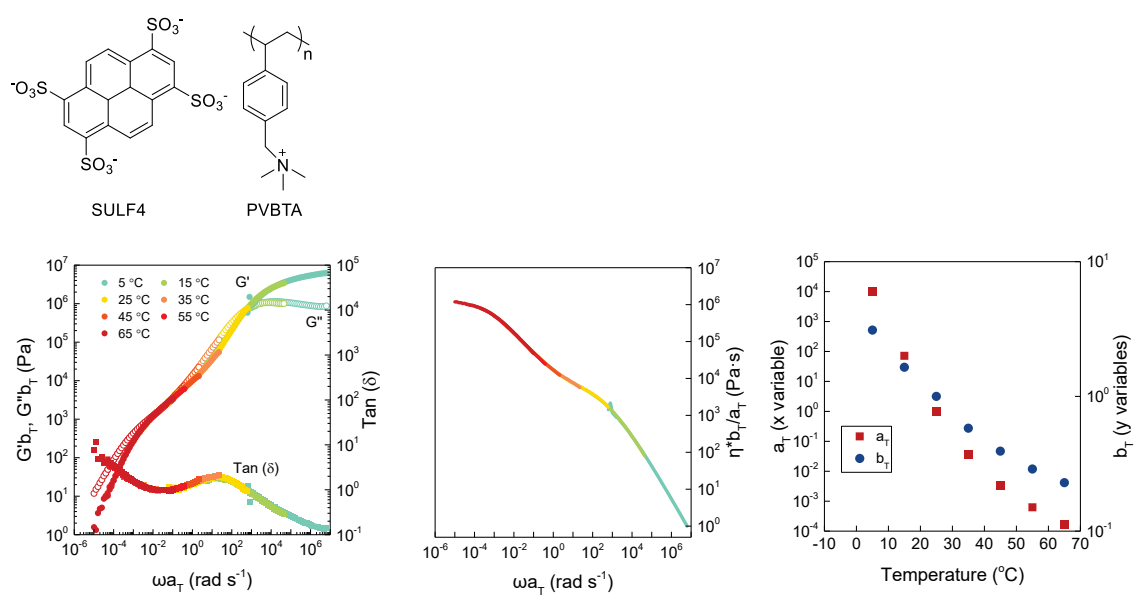


Fig. S5. Time-temperature superposition of SULF4/PVBTA coacervate ($T_g \sim 25$ °C) in 0.01 M NaCl. Reference temperature is 25 °C.

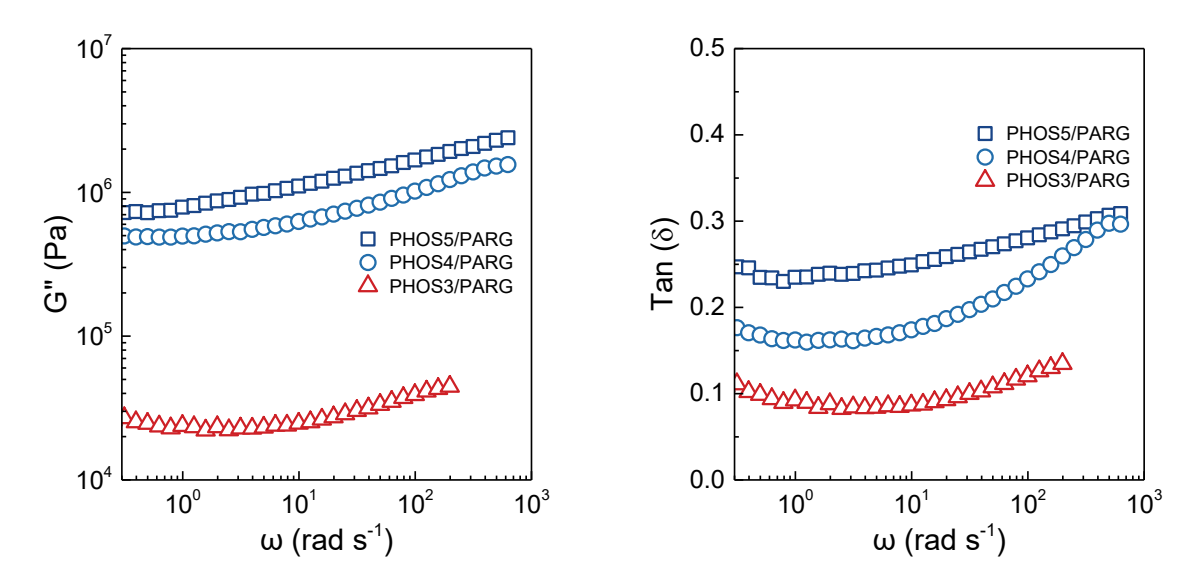


Fig. S6. G" and tano for PHOS/PARG series.

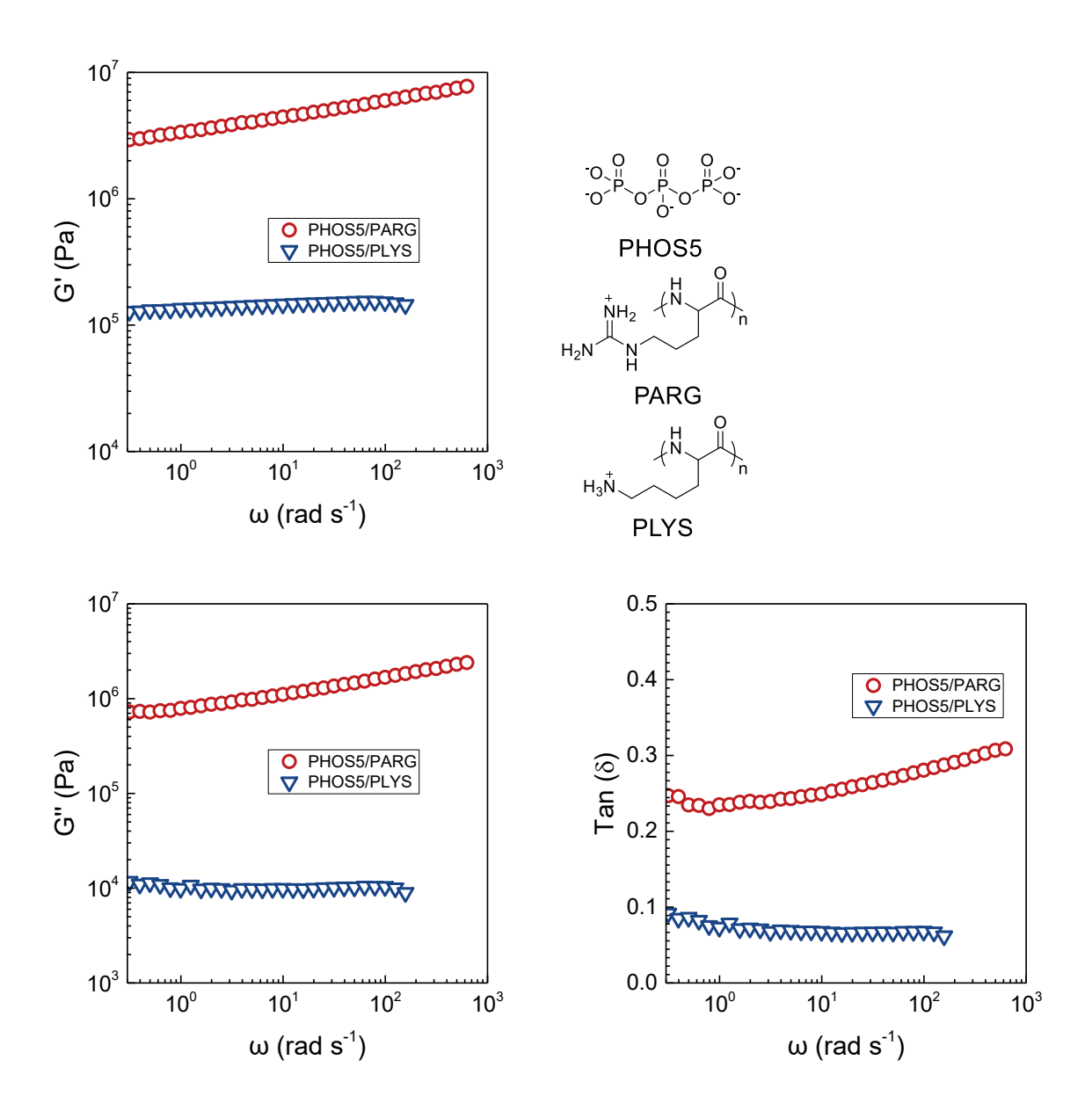


Fig. S7. G' versus frequency of \circ , PHOS5/PARG; ∇ , PHOS5/PLYS at 37 °C in 0.15 M NaCl, solution pH = 7. PARG forms more viscous coacervates.

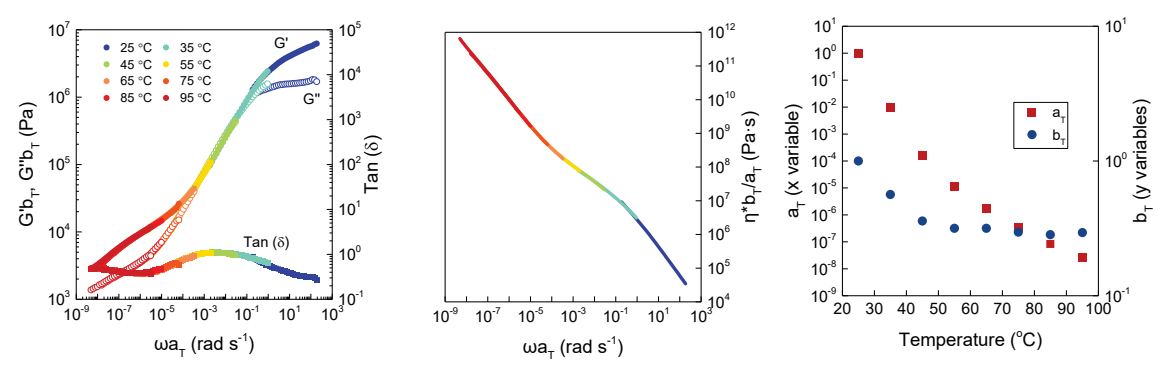


Fig. S8. Linear viscoelastic response of PSS/PDADMA using time temperature superposition. Reference temperature is 25 °C.

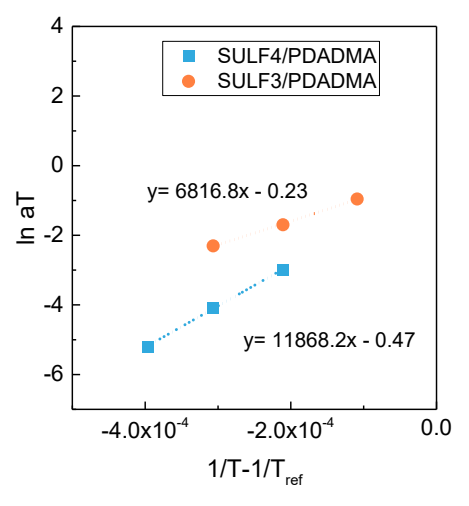
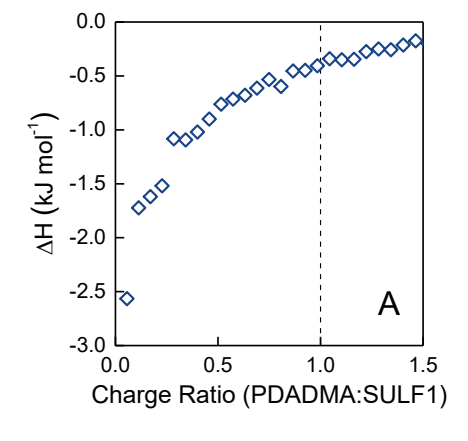
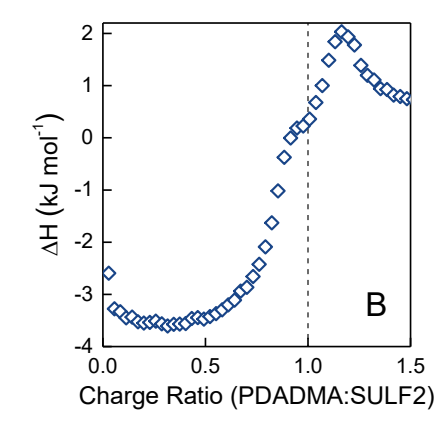
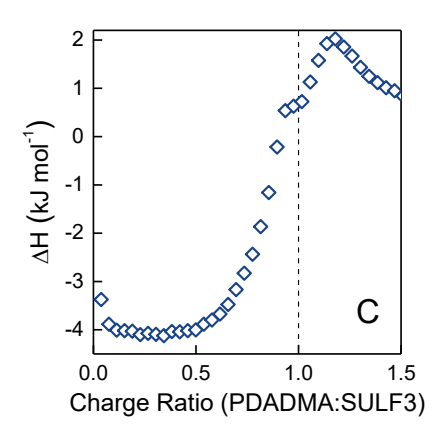


Fig. S9. Arrhenius plot of SULF4/PDADMA and SULF3/PDADMA. Activation energy, E_a , is obtained from the slope of the line, $E_a = 8.314 \times \text{slope}$. For SULF3/PDADMA, $E_a = 56.7 \text{ kJ}$ mol⁻¹, whereas for SULF4/PDADMA, $E_a = 98.7 \text{ kJ}$ mol⁻¹







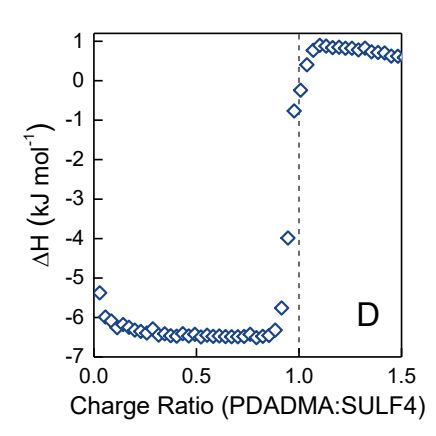


Fig. S10. Isothermal calorimetry titration curves. (A) 10 mM PDADMAC into 0.5 mM SULF1 in 0.05 M NaCl; (B) PDADMAC into 0.5 mM SULF2 in 0.05 M NaCl; (C) 10 mM PDADMAC into 0.25 mM SULF3 in 0.05 M NaCl; (D) 10 mM PDADMAC into 0.25 mM SULF4 in 0.05 M NaCl.